Original Research

Environment Friendly Synthesis of Novel Schiff Base-Derived Nano Metal Complexes Using Green Solvents for Enhanced Biological Activity

Maria Abdullah Butt[1], Sajid Rashid Ahmad[1], Muhammad Nawaz Chaudhary[2], Muhammad Zaheer[3]*, Rabia Nazir[3], Muhammad Zia-ur-rehman[3], Naqi Hussain[3]

[1]College of Earth and Environmental Sciences, University of the Punjab, Lahore-54000, Pakistan
[2]Department of Environmental Sciences and Policy, Lahore School of Economics, Lahore-53200, Pakistan
[3]Applied Chemistry Research Centre, Pakistan Council of Scientific and Industrial Research Laboratories Complex, Ferozepur Road, Lahore-54570, Pakistan

Abstract

This study uses an environmentally friendly approach to explore a new synthetic pathway for Schiff bases and their metal complexes. A new Schiff base ligand (C) was synthesized by reacting 7-aminodeacetoxycephalosporanic acid with benzaldehyde. The resulting Schiff base was then reacted with three transition metal (Zn, Fe, and Mn) nanoparticles facilitated by ethanolic extracts from three different plant leaves (*Moringa oleifera*, *Azadirachta indica*, and *Trigonella foenum-graecum*) to formulate environmentally friendly nanometal complexes (C1 to C9), which were subsequently evaluated for their anti-bacterial and antioxidant activities. These complexes exhibited crystallite sizes in the range of 7.24-64.24 nm. Structural, compositional, and elemental analysis of the Schiff base ligand and its metal complexes was carried out using FTIR, ^{1}H-NMR, ^{13}C-NMR, XRD, and SEM-EDX, which confirmed the integration of metal moieties within non-uniform sheet-like nanostructures. The thermal properties of all synthesized samples were quantified via TGA, which provides a comprehensive understanding of the thermal properties and decomposition mechanisms of Schiff bases and their metal complexes. Assessment of the antibacterial activity of the Schiff bases and their complexes revealed strong action against both gram-positive (*Staphylococcus aureus* and *Stenotrophomonas maltophilia*) and gram-negative (*Pseudomonas aeruginosa* and *Xanthomonas campestris*) strains. The prepared samples showed antioxidant activity in the following order: C4 > C5 > C6 > C1 > C2 > C3 > C7 > C8 > C9. Most of the samples, particularly the Zn-complex derived from Moringa, exhibit promising potential for pharmaceutical applications.

Keywords: Aldehyde, antimicrobial activity, antioxidant activity, green synthesis, monometallic complexes, plant extract

---

*e-mail: mzaheerchem@yahoo.com

Introduction

Recently, there has been significant research focused on the fabrication of nanostructured materials owing to their exceptional physical and chemical characteristics and their extensive range of practical applications. Likewise, the use of Schiff bases is experiencing rapid growth due to their diverse range and potential utilization in many diverse fields. In addition, complexes formed by combining Schiff bases with selected transition metals have recently been reported to exhibit noteworthy biological effects, including antimicrobial, antibacterial, antifungal, and anticancer properties [1–4].

The continual discovery of new and innovative compounds remains incredibly important. During the initial chemical revolution [5], the emergence of innovative and remarkable compounds not only fundamentally transformed contemporary existence concurrently but also engendered concerns about increased environmental pollution. Today, there is growing advocacy for industries to transition towards the initial synthesis of more environmentally benign chemicals and materials instead of enacting remedial measures for environmental restoration post-manufacturer to deal with a chemical contaminant. Furthermore, nanostructured Schiff base coordination complexes are industrially attractive due to their facile synthesis, broad chemical versatility, and multifaceted applications in materials chemistry, biological modeling, and catalytic processes. Green synthesis strategies that optimize drug development and utilize efficient and eco-friendly symbioses are also desirable. This leads to the development of crucial medicines. Environmental impact can be minimized by enhancing chemical processes through these methods. At present, significant efforts are being made to develop new multicomponent reactions (MCRs) and enhance existing reactions [6–8].

Metal nanoparticles can be made by using a variety of physical and chemical processes to achieve the desired physicochemical properties [9]. However, these traditional techniques are generally expensive, time-consuming, and harmful to the environment and living creatures due to the toxic chemicals they often use [10]. It is a scientifically settled fact that the use of many poisonous and hazardous solvents in organic synthesis threatens the health and safety of both chemists and the environment [11]. Thus, there is a pressing need to find an alternative, non-hazardous technique for the synthesis of nanoparticles. Green synthesis is one of the methods that employ biological agents like plant extracts for the synthesis of nanoparticles and is one such alternative.

While several biological processes may be employed to create nanoparticles of Schiff bases, plant extracts, which can function as both reducing and capping agents, are most often used in both small and large-scale nanoparticle synthesis [12–13]. Furthermore, biosynthetic production of nanoparticles using plant extracts is preferred since it is economical, environmentally friendly, requires only one step, and is safe for human therapeutic usage [14–15]. Precursor production of transition metal oxide Schiff base nanoparticles has recently seen widespread utilization of metal complexes and plant extracts [9].

For example, using 7-aminocephalosporanic acid as a starting point, a novel family of cephalosporin antibiotics was developed by altering the side chains at appropriate positions. Changes to the dihydrothiazine ring at position 3 affected pharmacokinetics and receptor binding affinity, whereas changes to the lactam ring at position 7 affected antibacterial activity [16]. However, particle size plays a pivotal role in determining drug solubility, and hence the fabrication of nanoscale Metal-Organic Frameworks (MOFS) has been proposed. The synthesis of the novel Schiff base ligand 7-ADCA (7-aminodeacetoxy ceflosporanic acid) and its nanocomplexes with transition metals using environmentally friendly solvents is proposed to circumvent toxicity and solubility issues and potentially decrease Pakistan's reliance on externally sourced antibiotics. These experiments could pave the way for creating more eco-friendly methods for synthesizing antibiotics.

Experimental

Materials

Ethanol, methanol, aldehyde, amino acids, and metal salts ($ZnSO_4.7H_2O$, $FeSO_4.7H_2O$, and $MnSO_4$) were acquired from Merck. All chemicals were analytical-grade. Commercial organic solvents were obtained from the local market and purified by means of industry standards (ethanol content of 94.9%) before use. Moringa plant (*Moringa oleifera*) leaves were collected from the Institute of Agriculture Science, University of the Punjab, Lahore, Pakistan, while Neem (*Azadirachta indica*) and Fenugreek (*Trigonella foenum-graecum*) plant leaves were obtained from the Pakistan Council of Scientific and Industrial Research Laboratories Complex, Lahore, Pakistan.
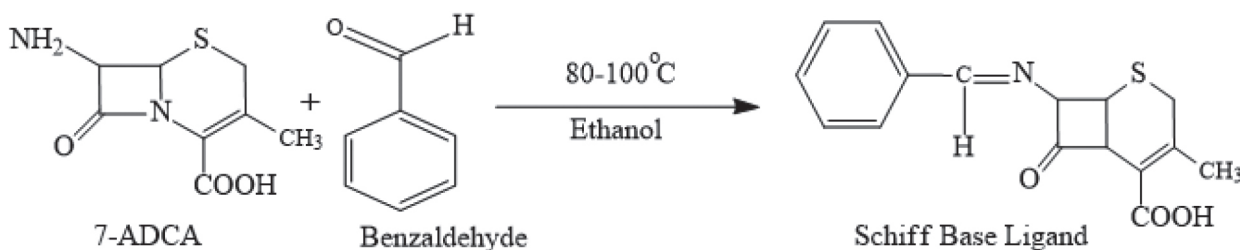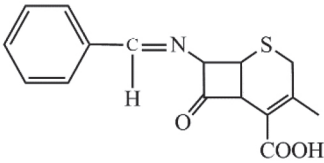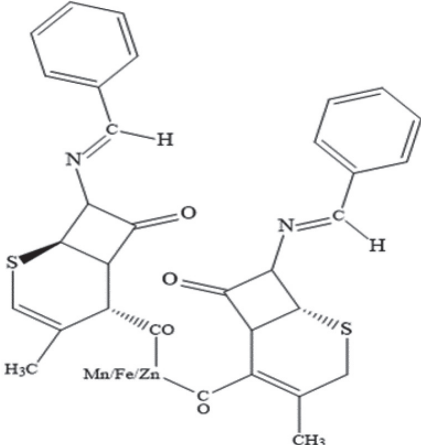

Fig. 1. Schiff Base Ligand 8-(benzylideneamino)-4-methyl-7-oxo-2-thiabicyclo [4.2.0] oct-4-ene-5-carboxylic acid

Table 1. Synthesis and yield percentages of Schiff base and its complexes with different transition metals

Complex	Sample Code	Yield % Percentage Yield= (Theoretical Yield/Actual Yield) ×*100*	Structure
Schiff Base	C	72	
C+AI+ Mn	C1	89	
C+MO+ Mn	C2	81	
C+TF+ Mn	C3	69	
C+AI+ Zn	C4	75	
C+MO+ Zn	C5	83	
C+TF+ Zn	C6	74	
C+AI+ Fe	C7	72	
C+MO+ Fe	C8	81	
C+TF+ Fe	C9	85	

AI = *Azadirachta indica;* MO = *Moringa oleifera;* TF = *Trigonella foenum-graecum*

Synthesis of Schiff Base Ligand (C)

The Schiff base ligand (C) was synthesized (Fig. 1) by adding 1 g 7-ADCA (7-Aminodeacetoxycephalosporanic acid) to 20 mL ethanol in a round bottom flask and stirring at room temperature with a magnetic stirrer. In this solution, 0.1mL of triethylamine (TEA) was added to dissolve 7-ADCA. After the dissolution, the reaction mixture was shifted to a water bath with heating at 80–100°C along with continuous stirring. In this reaction, 0.5 mL benzaldehyde was added dropwise, and the reaction continued for about 48 hours. After completion of the reaction, as confirmed by TLC using a chloroform-methanol (4:1) solvent system, ethanol was evaporated, followed by the addition of 50mL cold water, and stirred. After that, 0.15 mL sulfuric acid was added dropwise to precipitate the crude product, which was filtered, washed with cold water and dioxane three times, and dried at room temperature.

Plant-mediated Synthesis of Transition Metal Nanocomplexes

A one-pot method was adopted to synthesize the transition metal nanocomplexes of the prepared Schiff base. For this, three plants' leaves (*Moringa oleifera* (MO), *Azadirachta indica* (AI), and *Trigonella foenum-graecum* (TF), and three transition metals (Mn, Zn, and Fe) were employed, forming nine different Schiff base metal complexes (Table 1). The leaves of the plants were dried in the air and ground using a mortar and pestle. A total of 400 g of the powdered sample underwent extraction through cold maceration with 2L of ethanol. The resultant macerated mixture was then subjected to filtration and evaporation in a precise water bath at 50°C, resulting in the production of 27.2 g of a dark green semi-solid extract, which was carefully stored in a refrigerator at 4°C and later used for more applications by integrating the required quantity into ethanol. The ratio of drugs to metal sulfates was maintained at 1:2. The reaction contents (0.1 g metal sulfate, 0.2 g drug/ Schiff base, and 10 mL ethanolic solution of plant extract) were added to the Teflon autoclave. The contents were stirred at a magnetic stirrer for 30 min at room temperature and then autoclaved at 120°C for 6 hours. After that, the autoclave was cooled to room temperature, and the resultant Schiff base metal complex nanoparticle precipitates were filtered with a membrane filter, washed with ice-cold water and dioxane 3 times in a 1:1 ratio, and dried at room temperature [1–2]. Analytical data to prepared Schiff base metal complexes along with the Schiff base C is presented in Table 2.

Characterization

All the synthesized compounds were characterized using a range of different analytical, physicochemical, and spectral methods. Identification and quantification

Table 2. Analytical data of the nine prepared Schiff base metal complexes

Sample Codes	Name	Tentative Formula	Molecular weight (g mol^{-1})	Elemental Analysis (%)								Colour	mp °C
				C	H	N	O	S	Mn	Zn	Fe		
C	8-(benzylideneamino)-4-methyl-7-oxo-2-thiabicyclo[4.2.0]oct-4-ene-5-carboxylic acid	$C_{16}H_{15}NO_3S$	301.36	63.77	5.02	4.65	15.95	10.64	-	-	-	Orange	186
C1	((1R,5S)-8-((E)-benzylideneamino)-4-methyl-7-oxo-2-thiabicyclo[4.2.0]oct-3-ene-5-carbonyl)((1R)-8-((E)-benzylideneamino)-4-methyl-7-oxo-2-thiabicyclo[4.2.0]oct-4-ene-5-carbonyl)manganese	$C_{32}H_{28}MnN_2O_4S_2$	623.64	61.63	4.53	4.49	10.26	10.28	8.81	-	-	Dark Orange	171
C2												Dark brown	168
C3												Redish brown	166
C4	((1R,5S)-8-((E)-benzylideneamino)-4-methyl-7-oxo-2-thiabicyclo[4.2.0]oct-3-ene-5-carbonyl)((1R)-8-((E)-benzylideneamino)-4-methyl-7-oxo-2-thiabicyclo[4.2.0]oct-4-ene-5-carbonyl)zinc	$C_{32}H_{28}N_2O_4S_2Zn$	634.09	60.61	4.45	4.42	10.09	10.11	-	10.31	-	Yellowish green	182
C5												Blackish green	180
C6												Yellowish green	176
C7	((1R,5S)-8-((E)-benzylideneamino)-4-methyl-7-oxo-2-thiabicyclo[4.2.0]oct-3-ene-5-carbonyl)((1R)-8-((E)-benzylideneamino)-4-methyl-7-oxo-2-thiabicyclo[4.2.0]oct-4-ene-5-carbonyl)iron	$C_{32}H_{28}FeN_2O_4S_2$	624.55	61.54	4.52	4.49	10.25	10.27	-	-	8.94	Rust	179
C8												Blackish brown	180
C9												Blackish brown	183

of elements arising from the synthesis pathway were carried out through NMR using a Bruker Advance III HD 400 MHz NMR, equipped with TopSpin 3.5 software. It was also used for the structural elucidation of Schiff base ligands. The surface morphology and chemical composition of the synthesized Schiff base ligand and its complex with transition metals were examined by SEM-EDX analysis using a Nova NanoSEM 450 field-emission scanning electron microscope (FE-SEM). Functional groups present within the raw Schiff base and its metal complexes were identified using Fourier transform infrared spectroscopy (FTIR) over a range of 4000–600 cm^{-1} using Tensor-27. The crystalline nature and phase of the samples were investigated using an X-ray Diffractometer (Bruker, D2-Phaser). The melting point of the complexes was determined using electrothermal melting point equipment. Thermogravimetric analysis (TGA) was carried out using TGA 5500 equipment.

Antimicrobial Activity

Four bacterial strains, i.e., *Staphylococcus aureus, Stenotrophomonas maltophilia* (gram-positive), *Pseudomonas aeruginosa,* and *Xanthomonas campestris* (gram-negative), were used to determine the antibacterial efficiency of the prepared Schiff base and its metal complexes using standard procedures [17]. The ability of the Schiff base complexes to inhibit the growth of bacteria was compared against the known standard antibacterial drug, Cefradine. The well diffusion method was used to determine the bio-activity and sensitivity of compounds against pathogenic microorganisms, and these experiments were done in duplicate. The antibacterial activity was calculated after 24 hrs by measuring the zone of inhibition in mm [18].

Total Antioxidant Activity

The total antioxidant activity of Schiff base and its derivatives was measured through the development of a phosphomolybdenum complex by adopting a method developed by Prieto et al. [19]. In individual capped vials, every test compound and the standard Cefradine were dissolved in methanol at a concentration of 0.5 mg/mL^{-1}.Next, a freshly prepared phosphomolybdenum reagent solution (4 mL) was added to these solutions. (The reagent solution was produced by dissolving ammonium molybdate (2470 mg), sodium phosphate (5320 mg), and concentrated sulfuric acid (16.7 mL) in distilled water (500 mL). All the vials that contained the test compounds were then incubated for 70 minutes in an incubator set at 55 ± 1°C. A similar blank was also examined following the same procedure, without the addition of the test compound. After the incubation period, all vials were chilled to room temperature, and the absorbance for the test solutions, standard, and blank was measured using a UV-Vis spectrophotometer at 695 nm [20]. The total antioxidant potential of the derivatives was expressed relative to BHT (1.218). To confirm precision, all measurements were conducted in triplicate, and the mean values are presented in Table 3.

Table 3. Antioxidant activity based on absorbance at 695 nm.

Sample Code	Total antioxidant activity ± SEM
C	0.480 ± 0.02
C1	0.975 ± 0.08
C2	0.923 ± 0.09
C3	0.720 ± 0.03
C4	1.998 ± 0.22
C5	1.032 ± 0.01
C6	0.982 ± 0.12
C7	0.411 ± 0.29
C8	0.408 ± 0.14
C9	0.385 ± 0.03
Control BHT	0.46 ± 0.09

Results and Discussion

NMR Analysis

In the ^{1}H NMR spectra of the Schiff base ligand in Fig 2a, signals at $\delta = 8.27$ and $\delta = 7.18–8.85$ ppm were allocated to the hydroxyl protons of aromatics and amino protons (NH$_2$) [21]. The azomethine groups appeared in t between $\delta = 8.196–8.266$ ppm [22]. For the symmetrical Schiff bases, it was supposed to see only one chemical environment (as a singlet), but for the asymmetrical Schiff bases, two signals were seen. Aromatic ringed protons were revealed in the range of 7.1 to 8.45 ppm, and they were weakly affected by complexation [23–24]. Furthermore, it was stated that the special solvent molecule in the fifth position of the equatorial plane totally depends on the solvent that was used for the synthesis or recrystallization. It was confirmed that by changing the solvent of the synthesis or recrystallization, the coordinated solvent was changed. Furthermore, the ^{1}H NMR spectrum of the synthesized Schiff base metal complex showed amino (NH2) protons at $\delta = 4$ ppm as a singlet [21]. In addition, peaks at $\delta = 4.09–4.73$ are ascribed to the presence of CH$_2$-N and CH$_2$-O [25]. Therefore, the presence of a benzene ring in the Schiff base, along with the hydroxyl group in the azomethine moiety, participates in the development of intra-molecular resonance-stabilized H-bonds. The purity of the prepared ligand was detected by the disappearance of the hydroxyl group signal after the addition of D$_2$O.

The ^{13}C NMR spectrum of the synthesized Schiff base (Fig. 2b) showed the most de-shielded carbon peak present at 193 ppm, 171.29 ppm, $\delta = 171.5$ due to the carbonyl carbon shift in high and less conjugated systems [26]. The peak at $\delta = 164$ ppm is ascribed to an imine carbon, and this peak illustrates the presence of a carbon-carbon double bond [27]. The peaks between $\delta = 40$ and 50 ppm are due to aliphatic carbons, which include peaks due to
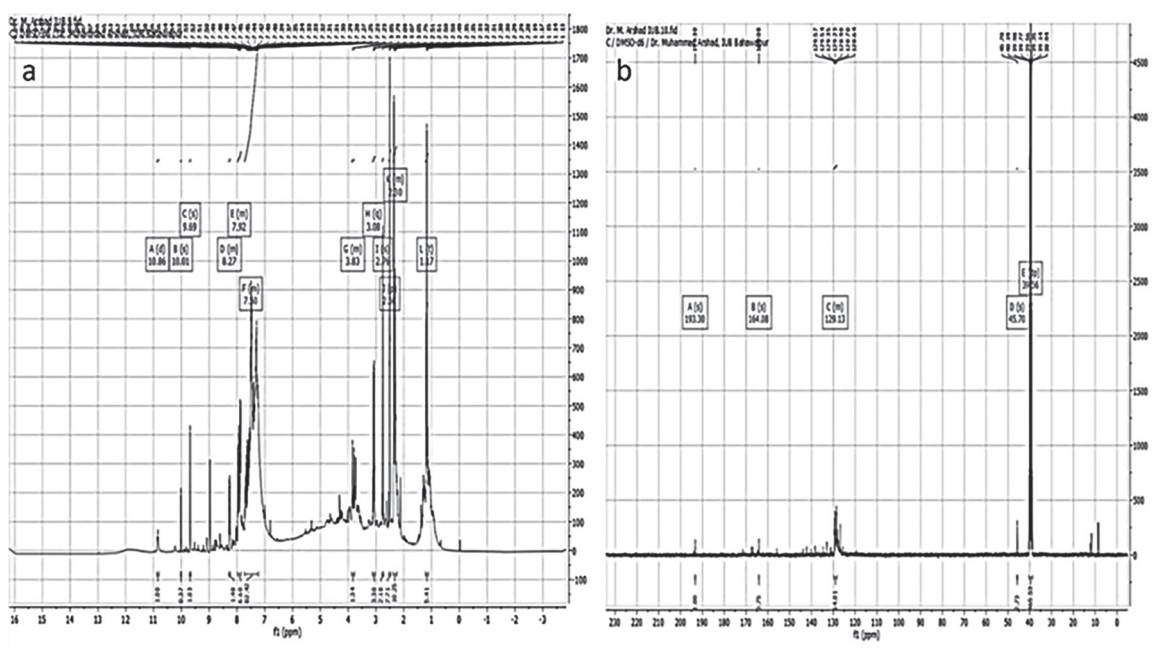
Fig. 2. ¹H-NMR (a) and ¹³C-NMR (b) spectra of the synthesized Schiff base.

solvent at δ = 45.5 ppm, indicating the presence of many carbon-carbon single bonds [21].

FTIR Analysis

Fourier Transform Infrared (FTIR) spectroscopy is an invaluable analytical tool used to discern the presence of distinct functional groups within chemical compounds. The FTIR spectra of all the samples (C-C9) are presented in Fig. 3. Sample C has several characteristic peaks. A broad peak spanning the range of 3300–2900 cm⁻¹ was attributed to the OH bond, while the peak at 2980 cm⁻¹ corresponds to the stretching vibration of the sp³ C-H bond. Additional peaks at 1607, 1214, and 1064 cm⁻¹ are ascribed to the C=N, C-O of carboxylic acid, and C=C bonds, respectively. The peak at 1448 cm⁻¹ is associated with the CH₂ bond (methylene).

Samples C1 to C3 exhibited additional peaks at 764 and 650 cm⁻¹ (associated with Mn-O and Mn-N bonds, respectively). Sample C4 showed overlapping OH and C-H peaks as a broad peak at 2924 cm⁻¹ and a characteristic peak at 1719 cm⁻¹ corresponding to the C=O of carboxylic acid [20]. Additionally, peaks at 1609, 1446, 1264, and 1069 cm⁻¹ were attributed to C=N, CH₂, and C-O bond vibrations. Samples C4 to C6 contained peaks at 631, 699, 634, 699, 634, and 628 cm-1 associated with Zn-O and Zn-N bonds, respectively.

Samples C7, C8, and C9 presented a different set of characteristic peaks, affirming the formation of Schiff base metal complexes as all complexes presented identical peaks. The observed peaks included 3211 cm⁻¹ (O-H bond), 1650 cm⁻¹ (C=N), 1438 cm⁻¹ (CH₂ group), and a range of peaks between 1300–1000 cm⁻¹ (C-O bond) [22]. Furthermore, peaks at 918 and 841 cm⁻¹ were attributed to Fe-OH bonds, while the peak at 636 cm⁻¹ was attributed to Fe-N bonds [23]. These findings contribute significantly to our understanding of the chemical composition and confirm the formation of Schiff base metal complexes [28].

XRD

The XRD patterns of the Schiff base (Fig. 4a) and its metal complexes (Fig. 4 b, c, and d) are sharp and crystalline, with the metal complexes having a very different XRD pattern from that of the ligand. Typically, due to the inherent crystalline structure of metallic compounds', crystallinity is often observed in metal-Schiff base complexes [29], but here, the small size of the diffraction peaks with broadening suggested a more amorphous structure. The XRD patterns of synthesized Schiff base (C) (Fig. 4a) have peak planes with hkl values of (202), (116), (211), (206), (140), (113), and (023) corresponding to angles of 18.1, 25.4, 26.7, 28.4, 34.8, 38.1, and 40.1°, respectively.

X-ray diffraction (XRD) patterns of C1 (Fig. 4b) exhibited two prominent peaks at 20.8° and 23.6°, corresponding to the crystallographic planes (100) and (220), respectively. Similar crystallographic plane peaks were observed at 20° and 25.5° for C2 and C3 (Fig. 4b) and are indexed to the manganese complex and are in good agreement with the reference patterns found in JCPDS Card No. 18-0802, which is standard birnessite-MnO₂ [1]. The XRD peaks for C2 and C3 exhibited heightened intensity and narrower profiles compared to C1, indicative of a greater degree of crystallinity.
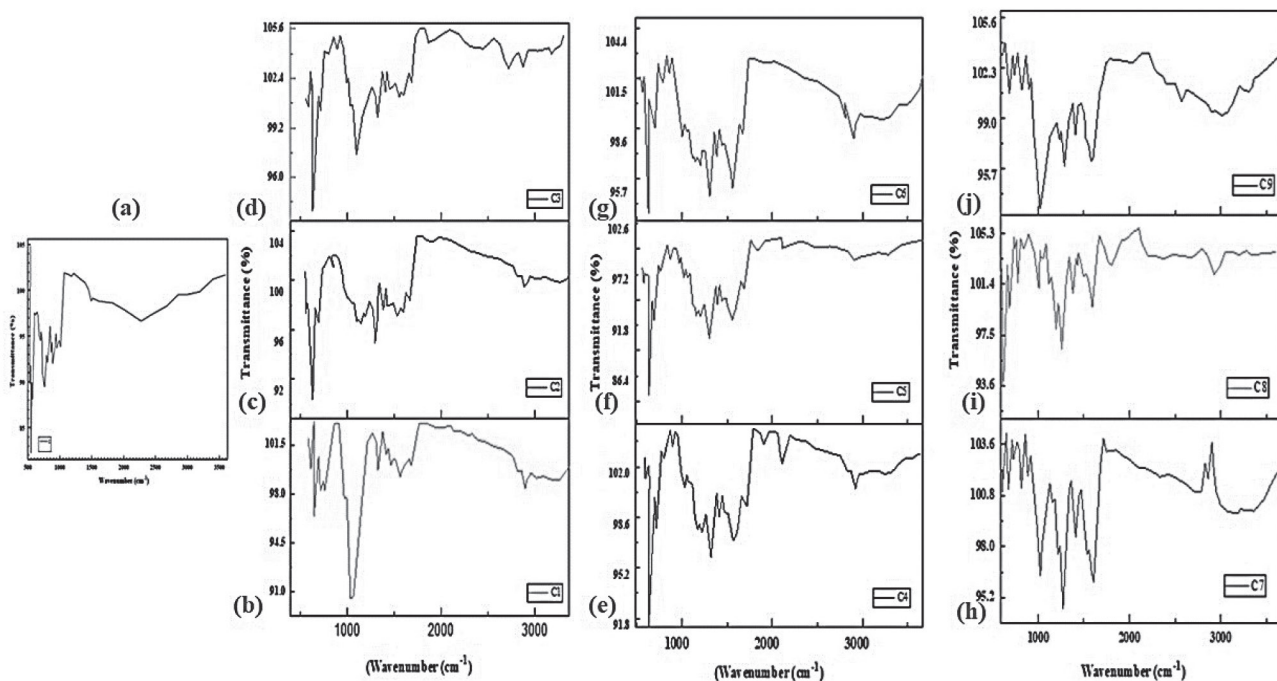
Fig. 3. FTIR spectra of Schiff base (a), and its metal complexes, C (a), C1 (b), C2 (c), C3 (d), C4 (e), C5 (f), C6 (g), C7 (h), C8 (i), C9 (j)
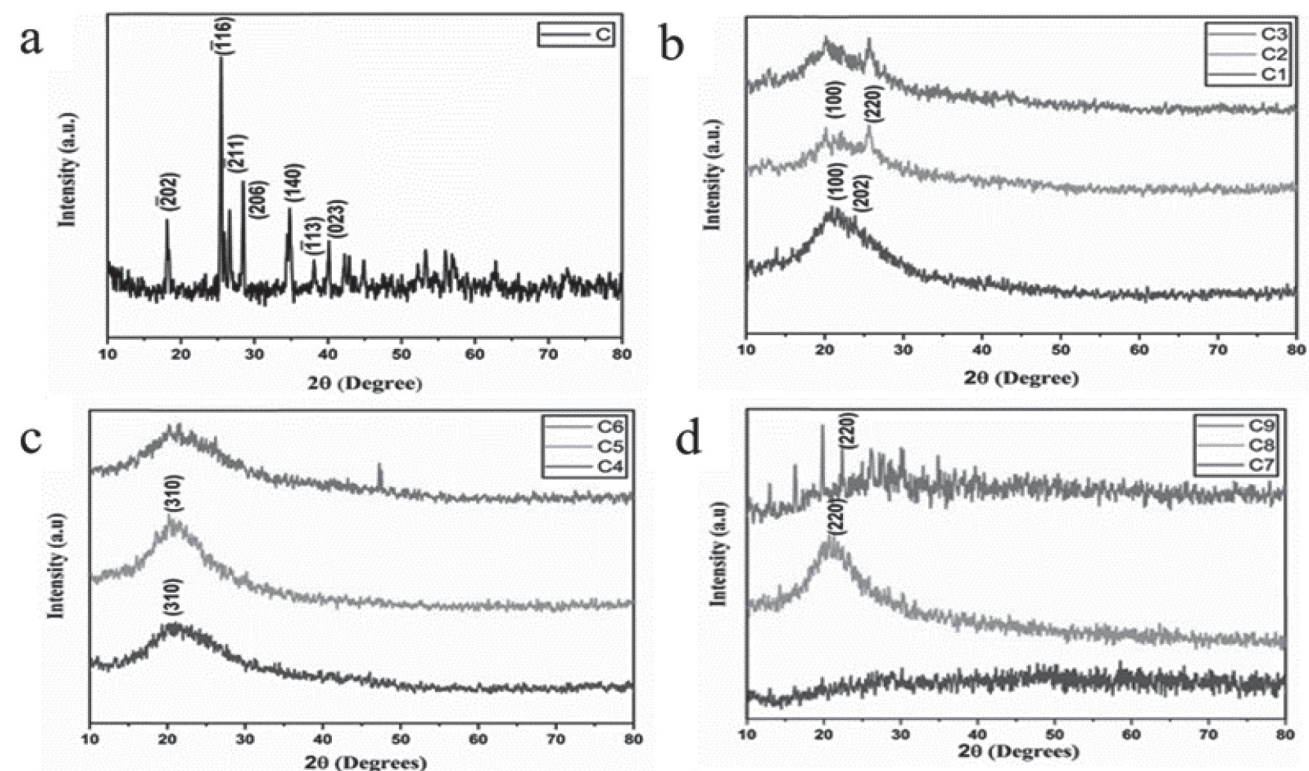

Fig. 4. XRD spectra of the Schiff base (a) and its metal complexes with Mn (b) (C1-C3), Zn (c) (C4-C6), and Fe (d) (C7-C9)

The XRD spectra (Fig. 4c) of the three Zn complexes (C4, C5, and C6) all exhibited broad peaks between 20° and 21.4°, which were attributed to hkl values of (310). Specifically, C4 and C5 display diminished peak intensity, indicating reduced crystallinity, which was attributed to variations in synthesis temperatures or sample concentrations but essentially synthesized the required product. Conversely, C6 had a relatively sharp peak at 47.1°, signifying the coexistence of both crystalline and amorphous components. These XRD patterns affirm the presence of Zn metal,

consistent with JCPDS card No. 79-0206, which is standard ZnO [30]. The observed peak broadening in the XRD spectra can be attributed to the coordination of water molecules, where previous research has correlated such broadening with heightened crystallinity in Zn (II) complexes [31].

The XRD spectra (Fig. 4d) of the three iron (Fe)-based Schiff base metal complexes (C7, C8, and C9) were dissimilar. For example, C7 did not exhibit the prominent peaks observed in C8 and C9, indicating that this sample had an amorphous nature and lacked any well-defined crystalline structures. In contrast, C8 and C9 displayed observable peak broadening, a phenomenon frequently attributed to the presence of water molecules. The peak planes showed hkl values of 220 for C7, C8, and C9 at 19.8 and 22.5°, coinciding with Fe_7S_8 (JCPDS card no. 25-0411), confirming the presence of specific crystalline facets [32]. The XRD data was also used to calculate the average crystalline size using the D-Scherrer equation (Eq. 1) [33].

$$D = {}^K\lambda/_\beta \cos\theta \qquad (1)$$

While D is the crystallite size in nm, $\lambda = 0.154$ nm for X-ray radiation, k is a shape factor equal to 0.93, θ is the peak position, and β is the full width at half maximum (FWHM). The average crystalline size of Schiff base (C) and metal complexes C1, C2, C3, C4, C5, C6, C8, and C9 came out to be 7.24 nm, 33.25 nm, 30.6 nm, 24.05 nm, 64.25 nm, 49.75 nm, 53.9 nm, 48.5 nm, and 60.65 nm, respectively, while C7 was amorphous in nature.

SEM Analysis

The surface morphology of the ligand and the associated metal complexes was examined using SEM. Due to the coordination of metal ions at the donor sites of the ligand, the SEM micrographs of the ligand and metal complexes differ significantly [34]. Schiff base metal complexes can be formed by the nitrogen (N) of the imine group (-C=N-), which acts as a donor site and aligns with or around the metal center. In certain cases, the carboxylic acid group (-COOH) may have oxygen as a donor site, which can aid in the coordination of metal ions in this complex. Schiff base metal complexes are structurally stable because they rely on the coordination of these atoms with the metal center. In addition, SEM images of the metal complexes showed appreciable changes in shape as the metal ions changed [34]. The SEM image of the pure Schiff base sample (C) (Fig. 5a) indicates the formation of spherical-shaped agglomerated nanoparticles [35].

C1, C2, and C3 are all Mn-based Schiff base metal complexes. The SEM image of C1 (Fig. 5c) indicated the formation of irregular shaped nanoparticles. In contrast, C2 showed two types of particles in the SEM image (Fig. 5e), i.e., particles having a nail-like structure and other particles having a sheet-like structure [36]. In comparison, the SEM image of C3 (Fig. 5g) indicated the formation of sheet-like structures [36]. Samples C4, C5, and C6 are Zn-based Schiff base metal complexes. The SEM image of C4 (Fig. 5i) showed the formation of irregularly shaped
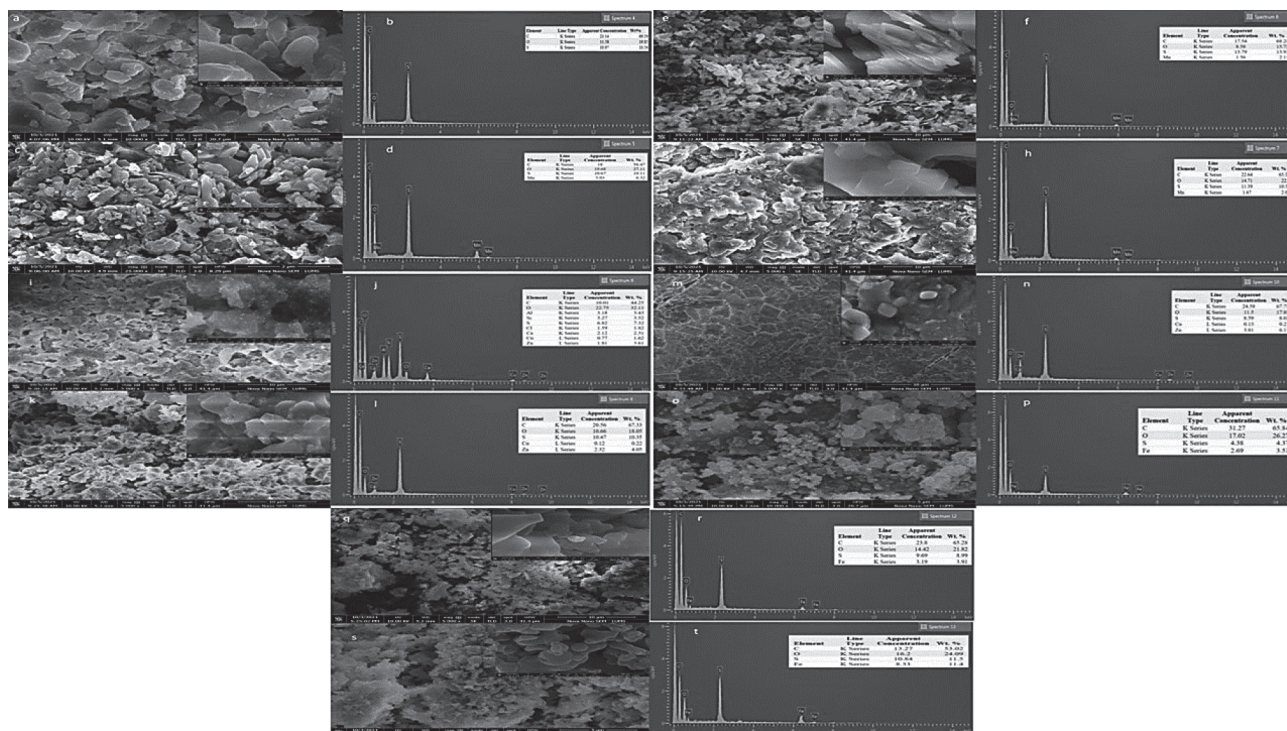

Fig. 5. Comprehensive morphological and elemental insights showing from left to right High-Resolution SEM Image, EDX image and elemental composition of Compound C (8-(benzylideneamino)-4-methyl-7-oxo-2-thiabicyclo [4.2.0]oct-4-ene-5-carboxylic acid). Morphological Evaluation and Elemental Profiling: SEM Micrographs and Quantitative EDX Analyses for Samples C1, C2, C3, C4, C5, C6, C7, C8 and C9.
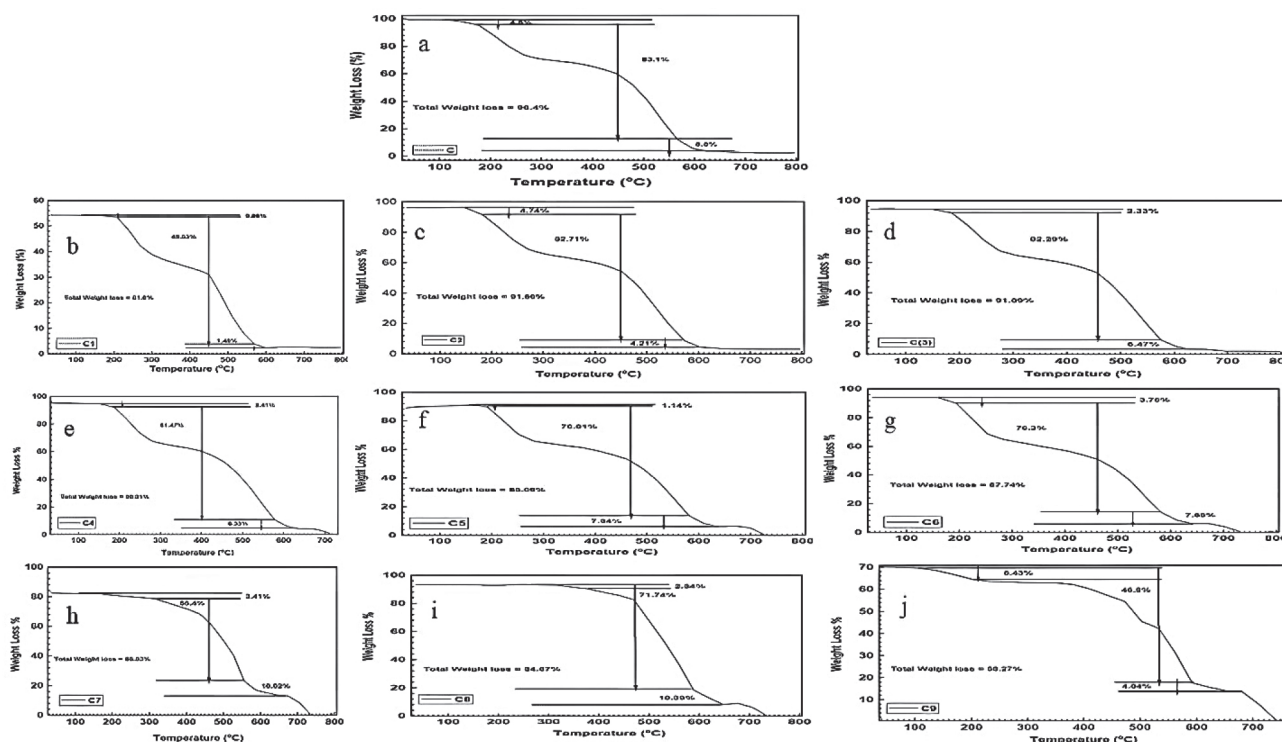
Fig. 6. Comprehensive thermogravimetric analysis (TGA) curves for Samples C-C9: Elucidating thermal decomposition profiles and weight loss dynamics over an extended temperature range of 100 to 800°C.

agglomerated sheet-like structures with an irregular distribution of particles, indicated by the formation of porous spaces on the surface [30]. The SEM image of C5 (Fig. 5k) shows agglomerates of two different regular shapes, i.e., square and spherical particles. In contrast, the morphology of C6 (Fig. 5m) was quite regular with square-shaped particles [37]. The SEM images of the Fe-based Schiff base metal complexes (C7, C8, and C9) are presented in (Fig. 5). The SEM image of C7 (Fig. 5o) shows the formation of agglomerated particles of different sizes [38]. The morphology of C8 was that of round-shaped plates carrying small aggregates with an almost uniform distribution of particles (Fig. 5q). The SEM image of C9 (Fig. 5s) depicted irregular agglomerated particles with few porous spaces.

Overall, the SEM analysis indicated that all synthesized metal complexes had an aggregated distribution. Furthermore, particle shape varied with the different metal Schiff base complexes, which were also different from the parent Schiff base. The variation in the morphology of the Schiff base metal complex crystal aggregates was mainly attributed to the different metal ions being deposited differently on the thin films. The nitrogen atom of the imine group of a Schiff base ligand can be joined to iron in alternating phases, creating atomic coordinate bonds. The ability of manganese to form coordinate bonds with nitrogen atoms in Schiff base ligands is like that of iron. Zinc, which has a coordination number of 4, typically forms coordination complexes with the nitrogen atom of the Schiff base ligand.

A pair of electrons are passed through the zinc atom to complete the coordination sphere.

EDX

Energy-dispersive X-ray (EDX) spectroscopy is an analytical technique that enables the chemical characterization of materials. Elemental mapping and composition of the synthesized Schiff base (C) surface (Fig. 5b) indicated the presence of only three major elements, i.e., C (69.56%), O (19.85%), and S (10.56%). In contrast, EDX indicated the presence of Mn in C1-C3 (Fig. 5d, f, h), Zn in C4-C6 (Fig. 5j, l, n), and Fe in C7-C9 (Fig. 5p, r, t), which also confirmed the successful synthesis of the metal-based Schiff base complexes.

TGA

The thermal stability of the parent Schiff base and its metal complexes were also examined by TGA [4]. Each TGA curve can be divided into three main regions according to the temperature and percentage weight loss. The decomposition of the organic components of these complexes can occur in one or more steps, potentially resulting in the formation of one or two intermediate products [39]. For metal complexes, these intermediate products consist of the metal ion combined with a portion of the Schiff base, which may ultimately undergo decomposition, leading to

Table 4. Inhibition Percentages of Antibacterial activity of C to C9 at two different doses and four pathogenic bacterial strains. All values are Mean ± RSD.

	12.5 mg/ml				25mg/ml			
	S. Aureus	*P. Aeruginosa*	*X. Campestris*	*Steno Maltophilia*	*S. Aureus*	*P. Aeruginosa*	*X. Campestris*	*Steno Maltophilia*
C	72.5 ±0.4	71.5±0.4	76 ±4	68.5 ±0.5	93 ± 0.8	93.5 ±0.7	97±0.3	94.5±0.6
C1	77.78±0.4	75.2±0.3	68.40±0.3	79.28±0.4	100±0.3	96.43±0.03	90.63±0.1	100±0.3
C2	77.78±0.4	76.21±0.3	66.40±0.3	77.78±0.4	100±0.3	96.43±0.03	90.63±0.1	100±0.3
C3	72.78±0.3	72.71±0.4	68.41±0.3	53.56±0.4	95±0.05	96.43±0.03	90.63±0.1	100±0.5
C4	73.45±0.3	73.71±0.4	75.79±0.4	68.78±0.2	95.67±0.4	96.43±0.03	98.01±0.02	90±0.1
C5	71.93±0.3	76.21±0.4	67.91±0.4	72.29±0.3	94.15±0.1	96.43±0.03	90.625±0.10	94.51±0.05
C6	72.28±0.3	71.71±0.4	66.41±0.3	65.45±0.3	94.5±0.1	96.43±0.03	90.625±0.10	90.165±0.1
C7	75.78±0.4	72.71±0.4	67.41±0.3	77.78±0.4	100±0.1	96.43±0.03	90.625±0.10	100±0.7
C8	75.28±0.5	71.71±0.4	66.91±0.3	75.78±0.5	100±0.2	96.43±0.03	90.6±0.1	100±0.1
C9	77.28±0.4	73.21±0.4	76.28±0.4	68.41±0.3	100±0.6	96.43±0.03	100±0.1	90.625±0.1

the formation of stable metal oxides. Thus, the decomposition of all these complexes ultimately resulted in the formation of stoichiometric oxides [2].

For C (Fig. 6a), in the first region, a weight loss of 4.8% were observed as the temperature increased from 104 to 176 °C. In the second region, total weight loss increased to 83.1%. as the temperature increased from 176 to 566°C. In the third region, a weight loss of only 8.5% was observed as the temperature increased from 566 to 625°C, and thereafter no further weight loss occurred, indicating the formation of a stable metal oxide with a residue mass of 8.5%. In certain instances, this elimination process can coincide with the partial oxidative degradation of the Schiff base, which may be the case here. Eventually, the organic ligand underwent decomposition, occurring either in one or two successive steps [40].

For the three Schiff base Mn complexes (C1, C2, and C3), total weight loss of 51.8, 91.66, and 91.09% was observed, respectively, in three gradual steps, which were assigned to the expected loss of $C_{10}H_{11}NO$ moieties and the phenylene group C_6H_4, leading to a decomposition step and Mn-metal oxide formation with residue weights of 1.8%, 4.21%, and 6.47%, respectively. For the three Zn Schiff base metal complexes (C4, C5, and C6), total weight loss was 90.21%, 85.09%, and 87.74%, respectively, leading to residual Zn oxide weights of 6.33%, 7.94%, and 7.68%, respectively [41]. For the Fe metal complexes (C7, C8, and C9), total weight loss was 68.83%, 84.67%, and 56.27%, respectively, which was attributed to the expected loss of the acetate group and a phenyl/naphthyl moiety at different temperatures, resulting in the formation of stable FeO residue weighing 10.02, 10.39, and 4.04%, respectively. Notably, all the anhydrous complexes exhibited a melting behavior prior to the onset of thermal decomposition, indicating a significant degree of covalent character in these compounds, which adopt tetrahedral stereochemistry [42].

Antibacterial Activity

The ability of the Schiff base "C" to inhibit the growth of pathogenic bacteria was compared to the antibacterial drugs Cefradine (positive control) and DMSO (negative control) [43]. The results demonstrated that Schiff base "C" and its metal complexes inhibited growth against all the tested bacterial strains, with varying degrees of effectiveness. Notably, the inhibition was concentration-dependent, i.e., higher concentrations showed greater inhibition. The trend of inhibition at lower concentrations was *Xanthomonas campestris > Staphylococcus aureus > Pseudomonas aeruginosa > Streptophomonas maltophilia*, while at higher concentrations, the trend was similar but with increased inhibition percentages [44]. Metal complexes of zinc (C4, C5, and C6) showed notable growth inhibition against specific pathogens, with zinc complexes demonstrating maximum inhibition against *Pseudomonas aeruginosa*. Manganese complexes exhibited different trends at lower and higher concentrations, with varying effectiveness against different pathogens, as observed in Table 4, which illustrates that in the inhibition power of complexes is reduced at lower concentrations while the power is increased with growing concentrations. Iron complexes (C7, C8, and C9) displayed maximum growth inhibition against *Staphylococcus aureus* [3]. Overall, the synthesized Schiff base and its metal complexes display significant antibacterial activity, particularly at higher concentrations, suggesting potential for their use as antibacterial agents. The concentration-dependent effect suggests that the metal ion may disrupt bacterial cell processes, leading to increased antibacterial activity [45]. Conclusively, this study highlights

the potential antibacterial properties of Schiff base "C" and its metal complexes, with varying effectiveness against different pathogens. The concentration-dependent effect is noteworthy, indicating a promising avenue for further research and potential applications in antimicrobial therapies. The inhibition percentages of antibacterial activity of C to C9 at two different doses and four pathogenic bacterial strains are illustrated in Table 4.

Total Antioxidant Activity

Antioxidants are naturally occurring molecules that protect living organisms from the harmful effects of free radicals, but there are synthetic antioxidants. In response to free radicals, cells often naturally emit free radicals. Antioxidants are crucial in delaying or preventing the oxidation of easily oxidizable substances (substrates). Antioxidant compounds in living organisms protect free radicals from harming macromolecules and cells by interfering with them through free radical scavenging, enzymatic reactions, metal ion chelation, regulation of gene expressions, and quenching singlet oxygen [31]. Consequently, the search for antioxidants has assumed growing relevance in recent years. The current trend in antioxidant usage favors synthetic antioxidants over natural antioxidants since they tend to be more cost-effective and effective [46]. The phosphomolybdate approach has been extensively used to assess the total antioxidant activity of plant extracts. In the presence of extracts, Mo (VI) is changed to Mo (V), generating a phosphomolybdenium V complex with a green color and an absorbance maximum of 695 nm. Table 3 summarizes the antioxidant potential obtained for each sample, where a higher absorbance is indicative of higher antioxidant activity [47]. The Zn-complexes C4, C5, and C6 attained from Moringa, showed the highest antioxidant activity, whereas the Fe-complexes C7, C8, and C9 prepared using fenugreek had the poorest antioxidant activity. Comparatively, C1, C2, and C3 showed appreciable antioxidant activity.

Conclusion

This study has explored the possible ways for the eco-friendly synthesis of Schiff base and its metal complex nanoparticles. The comprehensive analysis conducted on the synthesis of the Schiff base and its transition metal nanocomplexes, and their characterization techniques has yielded valuable insights into the physical and chemical structure of synthesized complexes and their antioxidant and antimicrobial potential. The chemical structure of the Schiff base was determined by NMR spectroscopy. Fourier transform infrared spectroscopy (FTIR) was employed to identify the functional groups present in the Schiff base and its transition metal nanocomposites. X-ray diffraction (XRD) analysis confirmed the successful synthesis of the materials, as no additional peaks were observed, indicating high purity.

One notable aspect of our investigation was the examination of the biological activity of the nanocomposites, which showed that C4, C5, and C6 exhibited the highest antioxidant activity of all the samples, while sample C9 showed the lowest antioxidant activity. The data presented in this paper, particularly their confirmed chemical and physical structures, their biological activity against pathogenic strains, and their antioxidant competency, contribute to the growing body of knowledge in green chemistry, providing a sustainable pathway to produce nanocomposites (metal complexes) with reduced or zero impact on the environment. Nevertheless, it is crucial to identify the inherent limitations and challenges linked to any innovative strategy. Future research undertakings may emphasize refining green synthesis approaches, enhancing the scope of Schiff base metal complexes, and acknowledging possible applications across different scientific disciplines.

Conclusively, the green synthesis of Schiff base metal complexes illustrates a step forward in synchronizing scientific accomplishments in compliance with environmental accountabilities. The insights and principles extracted from this study provide a basis for ongoing advancements and explorations in sustainable chemistry, constructing a way for a highly sustainable and greener scientific landscape.

Conflict of Interest

The authors declare no conflict of interest.

References

1. DANG M.N., NGUYEN T.H., VAN NGUYEN T., THU T.V., LE H., AKABORI M., ITO N., NGUYEN H.Y., LE T.L., NGUYEN T.H. One-pot synthesis of manganese oxide/graphene composites via a plasma-enhanced electrochemical exfoliation process for supercapacitors. Nanotechnology, **31** (34), 345401, **2020**.
2. EL-BORAEY H., EL-GAMMAL O., ABDEL SATTAR N. Impact of gamma-ray irradiation on some aryl-amide-bridged Schiff-base complexes: spectral, TGA, XRD, and antioxidant properties. Journal of Radioanalytical and Nuclear Chemistry, **323**, 241, **2020**.
3. OMMENYA F., NYAWADE E., ANDALA D., KINYUA J. Synthesis, characterization and antibacterial activity of Schiff base, 4-Chloro-2-{(E)-[(4-fluorophenyl) imino] methyl} phenol metal (II) complexes. Journal of Chemistry, **2020**, 1, **2020**.
4. PATEL D.D., PATEL K. Ni (II) and Zn (II) Schiff base complexes: Synthesis, characterization and study of thermodynamic parameters and activation energy. Materials Today: Proceedings, **32**, 392, **2020**.

5. HRICKO J. Scientific rationality: Phlogiston as a case study. Elsevier, **2017**.

6. BANITABA S.H., SAFARI J., KHALILI S.D. Ultrasound promoted one-pot synthesis of 2-amino-4, 8-dihydropyrano [3, 2-b] pyran-3-carbonitrile scaffolds in aqueous media: A complementary 'green chemistry'tool to organic synthesis. Ultrasonics sonochemistry, **20** (1), 401, **2013**.

7. CHANDA A., FOKIN V.V. Organic synthesis "on water". Chemical reviews, **109** (2), 725, **2009**.

8. CHOI J.-W., SONG H.K., LEE W., KOO K.-K., HAN C., NA B.-K. Reduction of COD and color of acid and reactive dyestuff wastewater using ozone. Korean Journal of Chemical Engineering, **21**, 398, **2004**.

9. KATHIRESAN K., ALIKUNHI N.M., NABIKHAN A. In vitro synthesis of antimicrobial silver nanoparticles by mangroves, saltmarshes and plants of coastal origin. International Journal of Biomedical Nanoscience and Nanotechnology, **2** (3-4), 284, **2012**.

10. PATRA J.K., THATOI H.N. Metabolic diversity and bioactivity screening of mangrove plants: a review. Acta Physiologiae Plantarum, **33**, 1051, **2011**.

11. WAHAB A., HAIDER S.S., MAHMOOD I. Synthesis of Schiff bases from natural products and their remarkable antimicrobial and antioxidant activity. FUUAST Journal of Biology, **4** (1), 27, **2014**.

12. SAXENA A., TRIPATHI R., ZAFAR F., SINGH P. Green synthesis of silver nanoparticles using aqueous solution of Ficus benghalensis leaf extract and characterization of their antibacterial activity. Materials letters, **67** (1), 91, **2012**.

13. JAWOOR S.S., PATIL S.A., KUMBAR M., RAMAWADGI P.B. Green synthesis of nano sized transition metal complexes containing heterocyclic Schiff base: structural and morphology characterization and bioactivity study. Journal of Molecular Structure, **1164**, 378, **2018**.

14. BRAGA L., LEITE A.A., XAVIER K.G., TAKAHASHI J., BEMQUERER M., CHARTONE-SOUZA E., NASCIMENTO A.M. Synergic interaction between pomegranate extract and antibiotics against Staphylococcus aureus. Canadian journal of microbiology, **51** (7), 541, **2005**.

15. KAVITHA K., BAKER S., RAKSHITH D., KAVITHA H., YASHWANTHA RAO H., HARINI B., SATISH S. Plants as green source towards synthesis of nanoparticles. Int Res J Biol Sci, **2** (6), 66, **2013**.

16. GARCÍA-RODRÍGUEZ J., BELLIDO J.M., SÁNCHEZ J.G. Oral cephalosporins: current perspectives. International journal of antimicrobial agents, **5** (4), 231, **1995**.

17. DENG Y., LIM A., LEE J., CHEN S., AN S., DONG Y.-H., ZHANG L.-H. Diffusible signal factor (DSF) quorum sensing signal and structurally related molecules enhance the antimicrobial efficacy of antibiotics against some bacterial pathogens. BMC microbiology, **14** (1), 1, **2014**.

18. JUNAID M., YAN J., QI Z., HAROON M. Synthesis, characterization and antibacterial activity of ethylene diamine and 2-hydroxybenzadehyde Schiff base and its metal complexes. Journal of Chemistry and Environment, **1** (01), 5, **2022**.

19. PRIETO P., PINEDA M., AGUILAR M. Spectrophotometric quantitation of antioxidant capacity through the formation of a phosphomolybdenum complex: specific application to the determination of vitamin E. Analytical biochemistry, **269** (2), 337, **1999**.

20. RODRIGUES M., BENNEHALLI B., MANJAPPAIAH V.H., ANANTHA S. Synthesis, In-vitro Antioxidant, Anti-diabetic Evaluation and Docking Studies of Newly Synthesized Benzoxazole Derivatives. Trends in Sciences, **18** (21), 35, **2021**.

21. SUMRRA S.H., IBRAHIM M., AMBREEN S., IMRAN M., DANISH M., REHMANI F.S. Synthesis, spectral characterization, and biological evaluation of transition metal complexes of bidentate N, O donor Schiff bases. Bioinorganic chemistry and applications, **2014**, **2014**.

22. ALYAMANI N.M. New Schiff Base–TMB Hybrids: Design, Synthesis and Antiproliferative Investigation as Potential Anticancer Agents. Symmetry, **15** (3), 609, **2023**.

23. YEAP G.-Y., OSMAN F., IMRIE C.T. Non-symmetric chiral liquid crystal dimers. Preparation and characterisation of the (S)-(benzylidene-4′-substitutedaniline)-2 ″-methylbutyl-4‴-(4 ″″-phenyloxy)-benzoateoxy) hexanoates. Journal of Molecular Structure, **1111**, 118, **2016**.

24. RACZUK E., DMOCHOWSKA B., SAMASZKO-FIERTEK J., MADAJ J. Different Schiff bases—structure, importance and classification. Molecules, **27** (3), 787, **2022**.

25. KHALEFA O.S., MOHAMMAD A.-T. New Schiff base compounds with benzene moiety: FT-IR, 1H and 13C NMR Spectroscopy (1D) studies. Basrah Journal of Science, **38** (1), 98, **2020**.

26. KAMIŃSKI K., WIKLIK B., OBNISKA J. Synthesis and anticonvulsant activity of new N-phenyl-2-(4-phenyl-piperazin-1-yl) acetamide derivatives. Medicinal Chemistry Research, **24**, 3047, **2015**.

27. PRIYADHARSHINI N., IYYAM P., SUBRAMANIAN S., VENKATESH P.V. Synthesis, spectroscopic characterization and DNA interaction of schiff base curcumin Cu (II), Ni (II) and Zn (II) complexes. Pharma Chem, **7**, 186, **2015**.

28. TAI X., YIN X., CHEN Q., TAN M. Synthesis of some transition metal complexes of a novel Schiff base ligand derived from 2, 2'-bis (p-methoxyphenylamine) and salicylaldehyde. Molecules, **8** (5), 439, **2003**.

29. BULDURUN K., TURAN N., SAVCI A., ALAN Y., COLAK N. Synthesis, characterization, X-ray diffraction analysis of a tridentate Schiff base ligand and its complexes with Co (II), Fe (II), Pd (II) and Ru (II): Bioactivity studies. Iran. J. Chem. Chem. Eng. Research Article Vol, **41** (8), **2022**.

30. SHEIKHSHOAIE I., SHEIKHSHOAEI M., RAMEZAN-POUR S. Synthesis and characterization of nano sized ZnO and CdO by direct thermal decomposition of their nano sized metal Schiff base complexes. Chemical Methodologies, **2** (2), 103, **2018**.

31. AL ZOUBI W., AL-HAMDANI A.A.S., KASEEM M. Synthesis and antioxidant activities of Schiff bases and their complexes: a review. Applied Organometallic Chemistry, **30** (10), 810, **2016**.

32. YAO W.T., ZHU H.Z., LI W.G., YAO H.B., WU Y.C., YU S. H. Intrinsic peroxidase catalytic activity of Fe7S8 nanowires templated from [Fe16S20]/diethylenetriamine hybrid nanowires. ChemPlusChem, **78** (7), 723, **2013**.

33. DE A.K., MURDOCK D.C., MATAYA M.C., SPEER J.G., MATLOCK D.K. Quantitative measurement of deformation-induced martensite in 304 stainless steel by X-ray diffraction. Scripta materialia, **50** (12), 1445, **2004**.

34. SHAKIR M., HANIF S., SHERWANI M.A., MOHAMMAD O., AL-RESAYES S.I. Pharmacologically significant complexes of Mn (II), Co (II), Ni (II), Cu (II) and Zn (II) of novel Schiff base ligand,(E)-N-(furan-2-yl methylene) quinolin-8-amine: Synthesis, spectral, XRD, SEM, antimicrobial, antioxidant and in vitro cytotoxic studies. Journal of Molecular Structure, **1092**, 143, **2015**.

35. GAWANDE M.B., BONIFÁCIO V.D., LUQUE R., BRANCO P.S., VARMA R.S. Benign by design: catalyst-free in-water, on-water green chemical methodologies

in organic synthesis. Chemical Society Reviews, **42** (12), 5522, **2013**.

36. FELICELLI A., KATSAMBA I., BARRIOS F., ZHANG Y., GUO Z., PEOPLES J., CHIU G., RUAN X. Thin layer lightweight and ultrawhite hexagonal boron nitride nanoporous paints for daytime radiative cooling. Cell Reports Physical Science, **3** (10), **2022**.

37. KURAKULA M., EL-HELW A., SOBAHI T.R., ABDE-LAAL M.Y. Chitosan based atorvastatin nanocrystals: effect of cationic charge on particle size, formulation stability, and in-vivo efficacy. International journal of nanomedicine, 321, **2015**.

38. CHEN D., YANG B., JIANG Y., ZHANG Y.Z. Synthesis of Mn3O4 nanoparticles for catalytic application via ultrasound-assisted ball milling. ChemistrySelect, **3** (14), 3904, **2018**.

39. ABDEL-LATIF S., HASSIB H., ISSA Y. Studies on some salicylaldehyde Schiff base derivatives and their complexes with Cr (III), Mn (II), Fe (III), Ni (II) and Cu (II). Spectrochimica Acta Part A: Molecular and Biomolecular Spectroscopy, **67** (3-4), 950, **2007**.

40. ZOUBI W.A., AL-HAMDANI A.A.S., KO Y.G. Schiff bases and their complexes: Recent progress in thermal analysis. Separation science and technology, **52** (6), 1052, **2017**.

41. VERMA S.K., SINGH V.K. [M {κ 2 S, S-S2C-piperazine-C2H4N= C (R)} n]{Co (III), Ni (II), Cu (II) or Zn (II)} complexes bearing pendant Schiff base moieties: spectral characterization, fluorescence, cyclic voltammetric and TGA/DTA study. Journal of Coordination Chemistry, **68** (6), 1072, **2015**.

42. NAGAJOTHI A., KIRUTHIKA A., CHITRA S., PARAMESWARI K. Fe (III) complexes with Schiff base ligands: synthesis, characterization, antimicrobial studies. Research Journal of Chemical Sciences ISSN, **2231**, 606X, **2013**.

43. SADIGOVA S., MAGERRAMOV A., ALLAKHVERDIEV M. Synthesis of Schiff bases and oxazolidines from 2-amino-4-phenylthiazole. Russian Journal of Organic Chemistry, **44**, 1821, **2008**.

44. NAEIMI H., MORADIAN M. Synthesis and characterization of nitro-Schiff bases derived from 5-nitro-salicylaldehyde and various diamines and their complexes of Co (II). Journal of Coordination Chemistry, **63** (1), 156, **2010**.

45. JAYABALAKRISHNAN C., NATARAJAN K. Ruthenium (II) carbonyl complexes with tridentate Schiff bases and their antibacterial activity. Transition Metal Chemistry, **27**, 75, **2002**.

46. WAN C., YU Y., ZHOU S., LIU W., TIAN S., CAO S. Antioxidant activity and free radical-scavenging capacity of Gynura divaricata leaf extracts at different temperatures. Pharmacognosy magazine, **7** (25), 40, **2011**.

47. SHAH S.S., SHAH D., KHAN I., AHMAD S., ALI U., RAHMAN A. Synthesis and antioxidant activities of Schiff bases and their complexes: An updated review. Biointerface Res. Appl. Chem, **10**, 6936, **2020**.